Optimal Zeeman-NQR Powder Lineshape Calculations for $3/2 \leqq I \leqq 7/2$*

Theresa Varty, R. Julian C. Brown, and Francis P. Temme
Department of Chemistry, Queen's University, Kingston, Ontario, Canada

Z. Naturforsch. **45a**, 550–558 (1990); received August 23, 1989

The powder lineshapes, associated with Zeeman-NQR $\Delta|m| = \pm 1$ transitions for half-integer spin from 3/2 and 7/2 are derived using an optimized (θ, ϕ) sampling algorithm for the intensity response. The $I = 3/2$ system is examined over the full asymmetry range, whereas the $I > 3/2$ lineshapes are calculated for $\eta \leqq 0.35$. The algorithm adopted is modelled on the concepts in the earlier NMR lineshape calculations of Alderman, Solum, and Grant**.

Key words: NQR, Zeeman, quadrupole, powder, lineshape.

Introduction

The characterisation of Zeeman perturbed NQR, Z-NQR, has been of interest since the 1950s and the classic work of Toyama [1] and others [2–4]. The reason for a continuous interest in the topic is linked to its inherent application in the precise determinations of the electric field gradient (EFG) asymmetry parameter, η, derived from the study of either single crystals [5], or microcrystalline powder specimens [6]. For half integer spins of $I > 3/2$, the related 'pure' NQR problems have been the subject of recent exact analytical solutions [7]. The use of energy moment expansions, and the solutions of quartic equations using the 'resolvent cubic' treatments, has provided exact analytic forms for the individual $I = 5/2$ and $I = 7/2$ NQR problems for arbitrary η. In addition, the form of solutions over Liouville space for two quadrupolar spins, i.e., $I = 3/2$ and 5/2, has been reported recently [8].

In the context of the former developments Creel [7] and Muha [9] have solved the $I = 3/2$ Z-NQR problem analytically for arbitrary η and specific orientation of the magnetic field H, to the microcrystallite principal axis system of the EFG tensor. Muha's treatment [9] is more general, as it includes the ratio of the Zeeman energy to the quadrupolar coupling constant explicitly in the analysis. However, for $I \geqq 5/2$ spins in practical applications of Z-NQR with $\eta < 0.25$, the perturbation treatment (i.e. with respect to effects of the weak Zeeman field) still provides a valid and more useful formulation of the problem for general half-integer values of I, as shown in the work of Brooker and Creel [10] and Bryant and Hacobian [6].

The inherent applications of Z-NQR arise from the need to separately determine $e^2 Q q h^{-1}$ and η parameters, for $I = 3/2$ or for $I = 5/2$ when the 3/2–5/2 transition is inacessible experimentally [11]; in addition, Z-NQR studies allow one to determine the direction of the principal axis (z) of the EFG tensor in a single crystal. Further development of the Z-NQR research field [12], and of 'pure' NQR from powder specimens in general, may well be more constrained than NMR, because of questions of the resonance inhomogeneity [13] and difficulties associated with using 'spin-locking' techniques in experiments involving powders [14, 15].

The purpose of the present paper is to report a further application of an optimized computational algorithm for spherical averaging that gives one in an efficient computational manner a reasonable estimate of the Z-NQR powder lineshape for the case of parallel static and radiofrequency fields. In studying the 'powder response' for general half-integer spin between 3/2 and 7/2 associated with Z-NQR at low asymmetry, we will naturally focus on the $1/2 \leftrightarrow 3/2$ pure quadrupole transitions. These features of the $I = 3/2$ case are computed for totally arbitrary η.

The work reported here represents both, an explicit application of an algorithmic optimization technique, originally development by Alderman et al. [16] for estimating NMR powder lineshapes, and an extension of the preliminary work on Z-NQR of powders presented in [6].

* Presented at the Xth International Symposium on Nuclear Quadrupole Resonance Spectroscopy, Takayama, Japan, August 22–26, 1989.

** J. Chem. Phys. **84**, 3717 (1986).

Reprint requests to Dr. R. J. C. Brown, Department of Chemistry, Queen's University, Kingston, Ontario, K7L 3N6, Canada.

0932-0784 / 90 / 0300-0550 $ 01.30/0. – Please order a reprint rather than making your own copy.

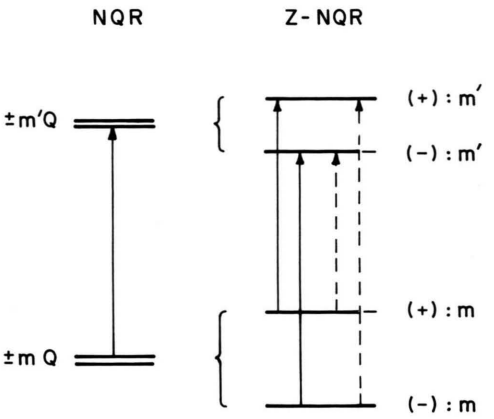

Fig. 1. The $\pm 1/2 \leftrightarrow \pm 3/2$ transitions of half-integer spins in NQR and Zeeman-perturbed NQR (Z-NQR). The labels $m, m' = m+1$ originating from NQR are taken as positive in both types of experiments. The Z-NQR frequencies that correspond to 'inner' and 'outer' pairs of transitions, are shown by (——) and (- - -) features, respectively.

Zeeman Perturbed NQR for Half-integer Spins

General Form of Powder Lineshape Calculation:

(A): The Hamiltonian and Energy Levels

In summarizing the salient points we will refer to the expressions derived by Toyama [1] and recently reconsidered in the work of Bryant and Hacobian [6].

The Hamiltonian

$$\mathscr{H} = (-) A \{3 I_z^2 - \boldsymbol{I}^2 + \eta [I_x^2 - I_y^2]\} - \gamma \boldsymbol{I} \cdot \boldsymbol{H}, \quad (1)$$

where $A = e^2 Q q h^{-1} / \{4 I (2I-1)\}$, includes a static magnetic term of the form

$$-\gamma H \{I_x \sin\theta \cos\phi + I_y \sin\theta \sin\phi + I_z \cos\theta\}. \quad (2)$$

Thus for H parallel to H_{rf} the problem is presented in (θ, ϕ) polar coordinates in the principal axis system of the nucleus within a representative microcrystallite. The perturbation treatment between pairs of degenerate states introduces diagonal terms M_{mm}, with $\cos\theta$ angular dependence of (9) of [6] and off-diagonal terms N_{mm}, between states $+m$ and $-m$ derived from $\{I_{x\,mm} \sin\theta \cos\phi \pm i\, I_{y\,mm} \sin\theta \sin\phi\}$, arising between the $\langle (\pm) m Q |$ and $| (\mp) m Q \rangle$ pure quadrupole states in (10) of [6].

Throughout the discussion, m is limited to positive values, and explicit external signs are shown where appropriate; this convention follows Toyama [1]. The transition moments $I_{\mu mm}$ are defined by

$$\begin{pmatrix} I_{x\,mm} \\ \pm I_{y\,mm} \end{pmatrix} = \langle \mp m Q | \begin{pmatrix} I_x \\ i I_y \end{pmatrix} | \pm m Q \rangle, \quad (3)$$

$$\begin{pmatrix} I_{x\,m(m+1)} \\ \pm I_{y\,m(m+1)} \end{pmatrix} = \langle \mp (m+1) Q | \begin{pmatrix} I_x \\ i I_y \end{pmatrix} | \pm m Q \rangle,$$

and

$$\begin{pmatrix} \pm I_{z\,mm} \\ \pm I_{z\,m(m+1)} \end{pmatrix} = \left\langle \begin{pmatrix} \pm m \\ \mp (m+1) \end{pmatrix} Q \middle| \, I_z \, | \pm m Q \right\rangle. \quad (4)$$

Their evaluation (to second order in η), and as a function of I is enumerated in the set of (21) of [1]. From these expressions it follows that the Zeeman-perturbed energy levels are

$$E_M = E_Q \pm [M_{mm}^2 + N_{mm} N_{mm}^{\dagger}]^{1/2}. \quad (5)$$

Thus the spherical coordinate dependence of the frequency shift is given by

$$E_M - E_Q = \pm \gamma H [I_{x\,mm}^2 \sin^2\theta \cos^2\phi + I_{y\,mm} \sin^2\theta \sin^2\phi + I_{z\,mm} \cos^2\theta], \quad (6)$$

as depicted for the 'inner' and 'outer' pairs of the $\Delta|m| = 1$ process of Toyama's presentation [1], as shown in Fig. 1; the 'outer' pair of frequencies arise purely from the application of the weak Zeeman field H and corresponds to a 'type I' calculation of [1] – the notation of Fig. 1 of [6] is not consistent with the original notation adopted in [1]. For $\Delta|m| = 1$ processes at low values of η, the $1/2 \leftrightarrow 3/2$ features of $I \geqq 3/2$ systems are those most strongly perturbed. As the 'type II' process is not consistent with the low η range for the quadrupolar spin $I < 7/2$ considered here, it will not concern us further.

The Formulation of the Intensity Aspects

The intensities $W_{EE'}$ for the $H \parallel H_{rf}$ problem arise from an expression

$$W_{EE'} \propto T^2 (EE')/h^2$$

involving the square of the transition moment, $T(EE')$, which includes the effect of the rf field components, $H_{r\,i}\,(i = x, y, z)$,

$$T^2 (EE') \sim \gamma^2 \sum_{\{ij\}} H_{r\,i} H_{r\,j} J_{ij} (E' E''). \quad (7)$$

Thus, the $J_{ij}(E' E'')$ intensity parameters depend on both $I_{\mu m' m''}$ and $I_{\mu m' m'}$ or $I_{\mu m'' m''}$ components. It is

convenient to write $F=1/(E_{m'}E_{m''})$ and

$$G_\mu = I_{\mu m' m'} I_{\mu m'' m''} H_\mu^2 \quad \{\mu = x, y\, z\},$$

so that the set of principal axis components are simply

$$\begin{aligned} 2J_{xx}(\pm) &= I^2_{x m' m''}\{1 \pm F(G_x + G_y + G_z)\}, \\ 2J_{yy}(\pm) &= I^2_{y m' m''}\{1 \pm F(-G_x - G_y + G_z)\}, \\ 2J_{zz}(\pm) &= I^2_{z m' m''}\{1 \pm F(-G_x + G_y - G_z)\}. \end{aligned} \tag{8}$$

The additional $J_{yz}(\pm)$ and related forms are also derived from the eigenfunctions of the Z-NQR with the rf terms included, so that

$$\begin{aligned} 2J_{yz}(\pm) = I_{y, m' m''} I_{z m' m''} \cdot \\ \cdot F H_y H_z \{-I_{y m' m'} I_{z m'' m''} - I_{z m' m'} I_{y m'' m''}\}; \end{aligned} \tag{9}$$

the remaining components are as given in Eqs. 17 (e)–17 (f) of [1]. This format of calculating the $J_{\mu\mu}(\pm)/J_{\mu\nu}(\pm)$ terms was adopted originally to allow for other experimental orientations of H relative to H_{rf}, with $I_{\mu m' m''}$ and $I_{\mu m m}$ corresponding to the rf and Zeeman transition moments, respectively.

The pairs of 'inner' and 'outer' pairs of transitions, shown in Fig. 1, correspond to the different signs of the $J_{ij}(\pm)$ components of the intensity calculation. The intensities of the lines that form a pair are identical, but the 'inner' and 'outer' pairs differ in their relative intensities. Only the 'type I' calculations of Toyama have been considered in these calculations for reasons discussed earlier.

Computational Aspects

It is generally convenient to consider the problem in a crystal reference frame and describe the orientation aspects in terms of θ and ϕ. Prior to the recent algorithmic methods, proposed by Alderman et al. [16], it was common to employ equal interval steps over a mesh of the (θ, ϕ) parameter surface together with the simple weighting factor $\sin\theta$; the disadvantages of such an approach from the point of view of optimal efficiency is that much of the time is spent evaluating mesh points of the (θ, ϕ) surface that make minimal contribution to the powder lineshape. In addition, repetitive calculations of trigonometric functions, as in the weighting process, are a major source of inefficiency in such calculations.

The computational aspects clearly need to be optimized to improve the accuracy associated with a specific number of computed steps, and/or over a given time interval. The axioms adopted in seeking such a rational optimization, both here and in [16], are as follows: (a) the partitioning of the (θ, ϕ) parametric surface must correspond to the selection of approximately equal solid angles; (b) that in handling adjacent (θ, ϕ) orientations, an efficient interpolation scheme is employed that collates the intensity responses in neighboring frequency regions in the same evaluation step; and finally, (c) that the direction cosines and related weighting functions are evaluated in terms of ratios of arithmetic forms, in place of explicit functions.

The interpolation technique implemented here is based on the use of a triangular grid of partitions over geometric space, as first utilized in [16]; a good choice of such a physical partitioning of the effective orientation interval comes from considering the $\{(x, 0, 0)/(0, y, 0)/(0, 0, z)\}$ triangular octant plane. The process of forming N^2 subdivisions then arises naturally from N divisions of each of the three (octahedral) edges associated with the specified plane and where the grid lines for the partitions are directed in directions parallel to these edges. For small triangles, a weighting function to allow both for variations in the solid angle subtended and for the cosine of the angle of tilt from the normal to triangular plane (from 0, 0, 0), still needs to be evaluated; this may be shown to be proportional to $(R')^{-3}$, where R' the distance of the plane from the origin.

The discrete representation of the amplitude of response over small frequency intervals is considered for the triangular grid in terms of a "tent" of amplitude versus frequency, as in diagram 2 (c) of [16]; both narrow "tents"-solely contributing in a single frequency channel – and broad "tents", spread over several channels, are possible. The full details of some ten cases inherent in the use of "tents" of $\{f_{min}, f_{mid}, f_{max}\}$ compared to axis $\{f_{low}, f_{high}\}$ values in the interpolation process are given in Alderman's original paper [16] and will not be repeated here. Naturally, each transition (line) of a rotation pattern will need to be considered in sequence to establish the full powder lineshape spectrum.

The direct evaluation of the direction cosines and polar coordinates in the optimized approach may be derived by using the indices i, j, and k corresponding to increments on the octant triangle's edges. The distance, R, between grid intersection and the octant origin is determined by $\sqrt{(i^2+j^2+k^2)}/N$; this param-

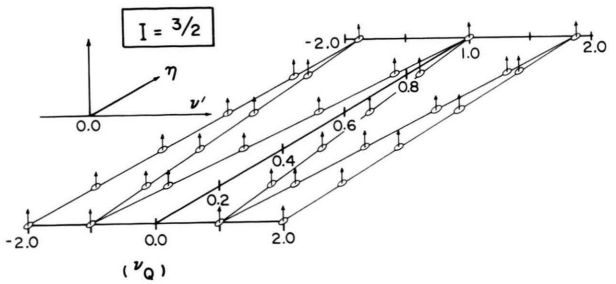

Fig. 2. A schematic diagram, indicating how the $I=3/2$ Z-NQR transition frequencies $\nu'=(\nu-\nu_Q)/\nu_0$ vary as a function of asymmetry, η. Analytical forms are available in earlier work [10], but the outline presented here provides a useful model with which $I=3/2$ lineshape features over η may be compared. The horizontal scale is the relative frequency shift ν'.

eter and the set of octant edge indices $\{i,j,k\}$ then allow one to formulate the direction cosines and angular functions.

Contrasting Behaviour of Spectral Features for 1/2–3/2 Transitions

(a) Spin 3/2 Lineshapes

The variation of the transition frequencies for the combined Z-NQR experiment as a function of η and (θ,ϕ) have been discussed in analytical form in the earlier work of Brooker and Creel [10] and Creel and Drabold [5]. Some of the general features of the dependence of the dimensionless frequency term $\nu'=(\nu-\nu_Q)/\nu_0$ on η, and on the (θ,ϕ) orientation, are shown schematically in Figure 2. For this *specific* case of $I=3/2$ the three 'critical points' or 'turning points',

$$\begin{aligned} &\theta=\pi/2, \quad \phi=0, \quad H\parallel(x),\\ &\theta=\pi/2, \quad \phi=\pi/2, \quad H\parallel(y),\\ &\theta=0, \quad\quad\quad H\parallel(z), \end{aligned} \tag{10}$$

exhibit the limiting behaviour

$$\begin{aligned} H\parallel\begin{pmatrix}x\\y\end{pmatrix}:\ \nu'\to\ &\pm1.86 \text{ and } 0.0 \text{ as } \eta\to1,\\ \nu'\to\ &\pm1.0, \text{ as } \eta\to0 \end{aligned} \tag{11}$$

and indicate that the $H\parallel z$ features near $\nu'=\pm2.0$ are not strongly η dependent. The features of the individual powder Z-NQR ($I=3/2$) spectra are shown in Fig. 3 with the typical gap forming about $\nu'=1.0$ as η departs from zero, and with the growth of a central peak and unsymmetrical side peaks at $\nu'=\pm1.86$, which form as $\eta\to1.0$.

(b) General Features of Z-NQR at $\eta=0$ for Spins $I>3/2$.

The origin of the $H\parallel\begin{pmatrix}x\\y\end{pmatrix}$ features for higher spins follow from the Bersohn-Toyama formulation with the following $\eta=0$ limits:

$$\begin{aligned} H\parallel\begin{pmatrix}x\\y\end{pmatrix};\quad &I=5/2:\ \nu'=1.5,\\ &I=7/2:\ \nu'=2.0,\\ &I=9/2:\ \nu'=2.5. \end{aligned} \tag{12}$$

The $H\parallel(z)$ condition is replaced, for $I=3/2$, by the conditions for the maxima of the function

$$\begin{aligned} &\nu'=1/2\,(\pm3\cos\theta\pm\sqrt{1+n'\sin^2\theta}) \qquad (13)\\ &\{n'=3,\ 8,\ 15,\ 24 \text{ for } I=3/2,\ 5/2,\ 7/2,\ 9/2\}, \end{aligned}$$

which implies that the outermost features correspond to orientations given by

$$\theta=\cos^{-1}\sqrt{(1+n')/\{n'(1+n'/9)\}}, \tag{14}$$

where n' is $\{(I+1/2)^2-1\}$.

In consequence, the critical maxima *replacing* the $H\parallel(z)$ feature for $I>3/2$ cases are now found at special angles $\bar{\theta}$ given by

$$I=5/2:\quad \bar{\theta}=\cos^{-1}0.7717_4, \tag{15}$$

$$I=7/2:\quad \bar{\theta}'=\cos^{-1}0.6324_5, \tag{16}$$

$$I=9/2:\quad \bar{\theta}''=\cos^{-1}0.4241. \tag{17}$$

These correspond to outer features at $\eta=0$, Fig. 4, at frequencies ν' as follows:

$$\begin{aligned} &I=5/2:\quad \nu'=2.19,\\ &I=7/2:\quad \nu'=2.56,\\ &I=9/2:\quad \nu'=2.91. \end{aligned} \tag{18}$$

Further details of these maxima are shown in Figs. 5 and 6 for $I=5/2$ and 7/2, respectively. The most obvious distinction between the $I=3/2$ and $I>3/2$ Z-NQR powder lineshapes arise from the low intensity at $\nu'=0$ for high spin, compared with the central maximum for $I=3/2$. The η variation of the lineshape for $I>3/2$ retains certain aspects of the $I=3/2$ model but the $H\parallel\begin{pmatrix}x\\y\end{pmatrix}$ features cross at $\nu'=0$ for $\eta=0.335$ ($I=5/2$) and 0.0185 ($I=7/2$) instead of at $\eta=1.0$ ($I=3/2$).

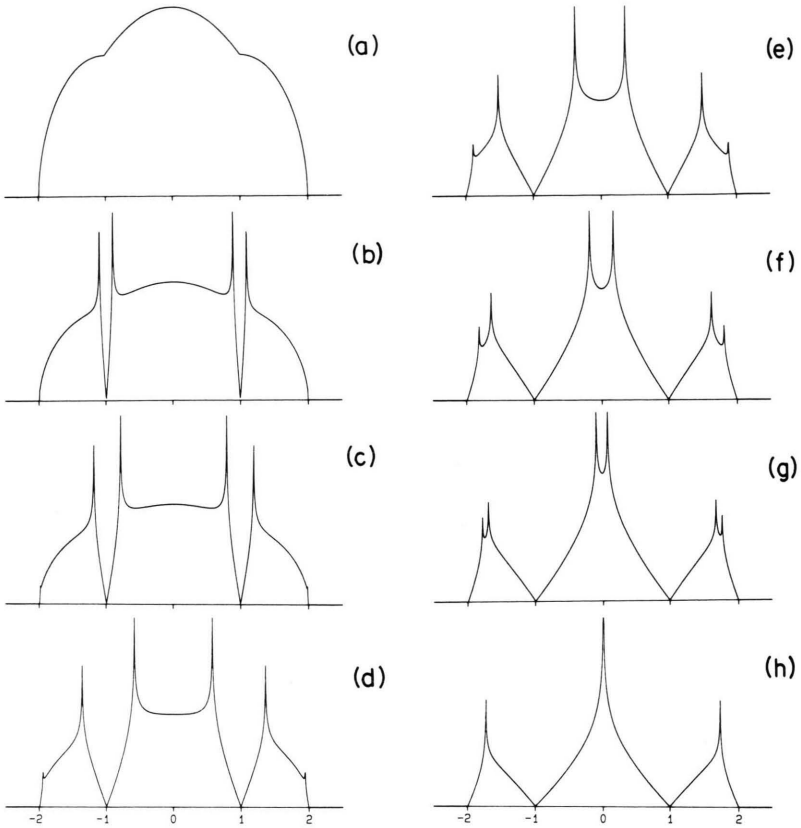

Fig. 3. The powder lineshapes for $I = 3/2$ and specific η values calculated by the optimized computational approach discussed in the text. The individual spectra correspond to $\eta = 0.0$, 0.1, 0.2, 0.4 and $\eta = 0.6$, 0.8, 0.9, 1.0 for 3 (a)–(d) and 3 (e)–(h), respectively.

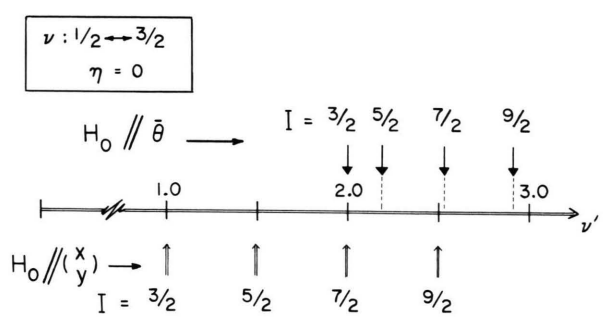

Fig. 4. Diagram summarizing features corresponding to both $H \parallel \begin{pmatrix} x \\ y \end{pmatrix}$ and $H \parallel \bar{\theta}$ orientations of the $\eta = 0$ spectra for different I spins. The special angle $\bar{\theta}$ for $I > 3/2$ is defined in the text and corresponds to the orientation of crystallites which contribute intensity at the other edges of the spectrum at $\eta = 0$.

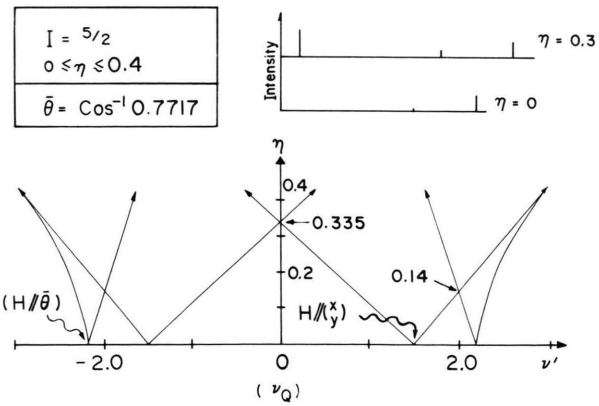

Fig. 5. The dependence of the $H \parallel \begin{pmatrix} x \\ y \end{pmatrix}$ and $H \parallel \bar{\theta}$ lineshape features on η for $I = 5/2$, showing the crossing of $H \parallel \begin{pmatrix} x \\ y \end{pmatrix}$ features at $\nu = 0$ at $\eta = 0.33_5$ and the crossing of the $H \parallel \bar{\theta}$ and $H \parallel \begin{pmatrix} x \\ y \end{pmatrix}$ frequencies at $\eta = 0.14$. The $H \parallel \begin{pmatrix} x \\ y \end{pmatrix}$ features meet at $\eta = 0$ with $\nu' = \nu'_{xy}$ given by (18). The inset illustrates schematically the changes of intensity of the features with η.

(c) Discussion of Specific $I \geqq 5/2$ Lineshapes for $\eta \leqq 0.4$

The computed lineshapes for $I=5/2$ over the range $0 \leqq \eta \leqq 0.4$, shown in Fig. 7, are now considered. The notable features in this region are the crossing of the inner $H \| \begin{pmatrix} x \\ y \end{pmatrix}$ branches at $\eta=0.335$, and the crossing of the outer branch of $H \| \begin{pmatrix} x \\ y \end{pmatrix}$ with another outer feature at $\eta \sim 0.135$. The full presentation of the η-dependence of the features is summarized in Figure 5. The intensity variation over η is also most marked with the outer $H \| \bar{\theta}$ component the strongest feature at $\eta=0$, whereas these features are only a weak pair of components at $\eta \sim 0.35$. For η between 0.30 and 0.34, the central $H \| \begin{pmatrix} x \\ y \end{pmatrix}$ feature is dominant. All the $I=5/2$ spectra in Fig. 7 exhibit sharp edges.

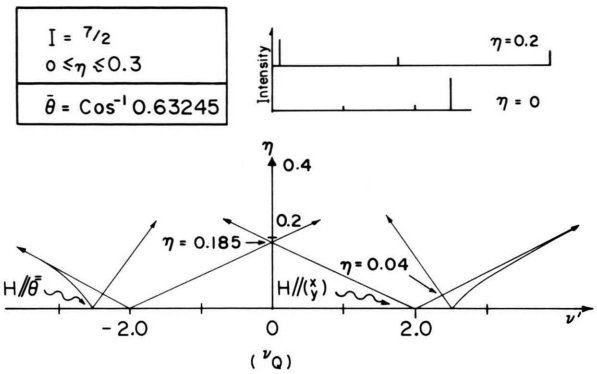

Fig. 6. Illustration of the frequency variations of the special features of the $I=7/2$ lineshape as a function of η. The sensitivity of $\nu'(\eta)$ to small changes in η is marked, as predicted by the Bersohn-Toyama slopes of Figure 9. Schematic intensity variations are shown in the insert.

The detailed lineshapes for $I=7/2$, as functions of η, are presented in Figure 8. The form of the $H \| \begin{pmatrix} x \\ y \end{pmatrix}$ dependence gives rise to the unusual spectral shape of Fig. 8 (f). This corresponds to a further inner $H \| \begin{pmatrix} x \\ y \end{pmatrix}$ 'crossing' phenomena similar to that seen in the $I=5/2$ spectra. The $H \| \bar{\theta}$ feature for $I=7/2$, which starts at $\nu'=2.56$ at $\eta=0$, becomes a weak feature at $\nu'=1.96$.

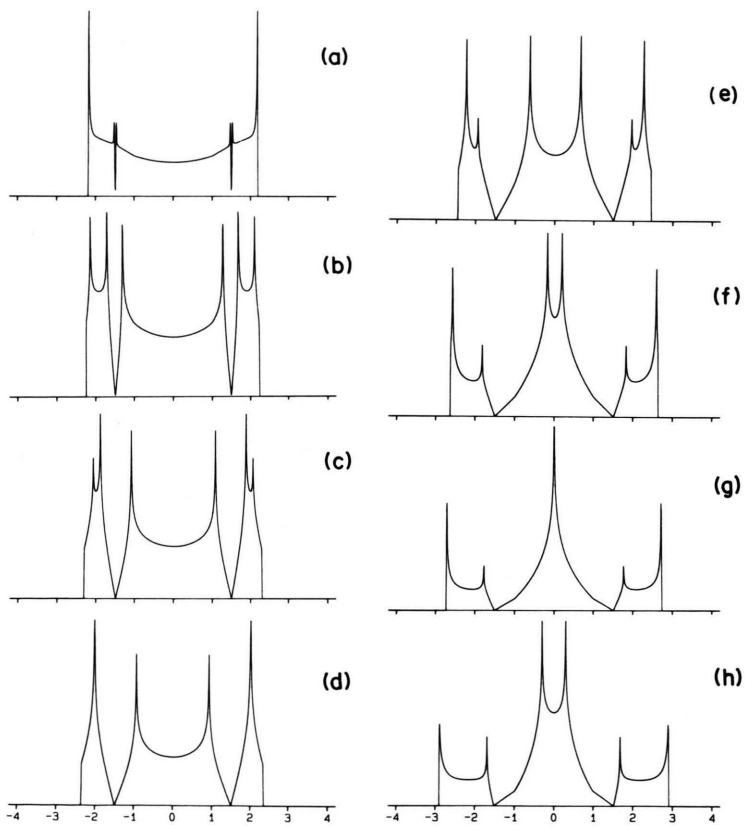

Fig. 7. The lineshapes associated with the $1/2 \leftrightarrow 3/2$ transitions of the spin $I=5/2$ for $0<\eta<0.40$ showing the $H \| \begin{pmatrix} x \\ y \end{pmatrix}$ features approaching $\nu'=0$ and 2.6 as $\eta \to 0.33_5$. The general $\nu'(\eta)$ dependence is shown in Figure 5. The specific η values associated with the specific lineshapes of illustrates 7(a)–(d) and 7(e)–(h) are 0.005, 0.05, 0.135, 0.2 and 0.25, 0.3, 0.335, 0.4, respectively.

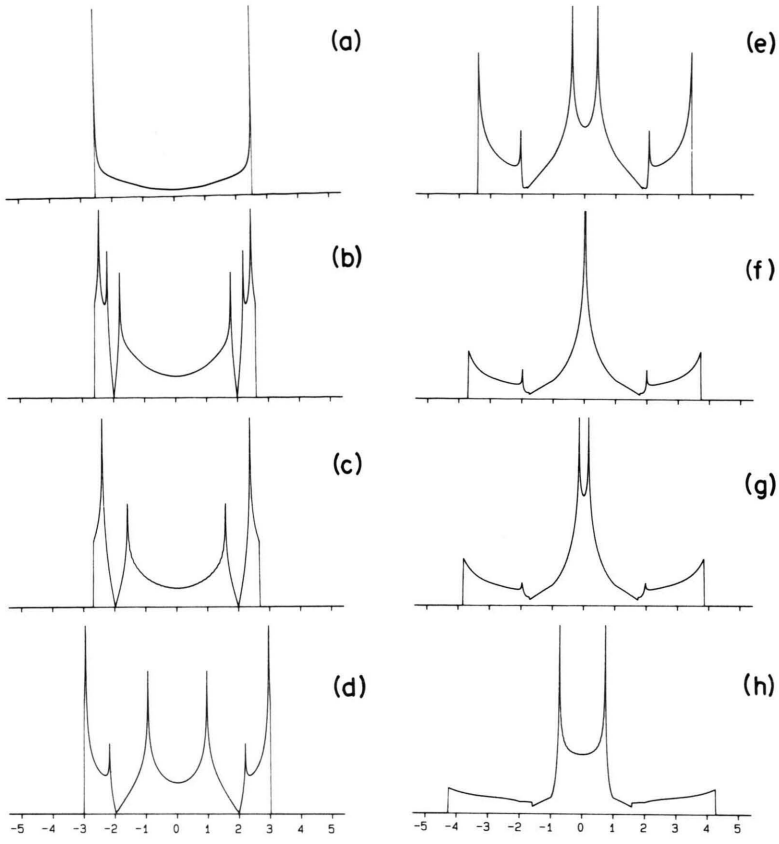

Fig. 8. The lineshapes of Z-NQR for $I=7/2$ for $0<\eta<0.25$, showing ν' of the $H \parallel \begin{pmatrix} x \\ y \end{pmatrix}$ features approaching 0 and 3.85 as $\eta \rightarrow 0.18_5$. The general $\nu(\eta)$ dependence of the $H \parallel \begin{pmatrix} x \\ y \end{pmatrix}$ features is shown in Figure 9. The specific η values shown are 0.00, 0.02, 0.04 and 0.10 in Figs. 7(a)–(d) and 0.15, 0.185, 0.2 and 0.25 in 7(e)–(h).

The detailed η dependence for $I=7/2$ is summarized in Figure 6. It is seen that the outer features corresponding to $H \parallel (\bar{\theta})$ are found at $\nu'=2.56$ for $\eta=0$. The major features cross at $\nu'=0.0$ when η reaches the value 0.185. An additional merging of outer spectral lineshape features occurs at $\eta=0.04$. Clearly, the powder lineshapes derived from Z-NQR of higher I nuclei are much more strongly dependent on η than are the lineshapes for $I=3/2$.

In Fig. 9 we show the initially linear dependence of the $H \parallel \begin{pmatrix} x \\ y \end{pmatrix}$ features as function of η with the $\eta=0$ origins of Fig. 4 shifted to a common reference origin. The behaviour with increasing half-integer I follows the form of the Bersohn-Toyama expression with their predicted departures from linearity for increasing η, as shown by the circles in Figure 9.

For applications that involve determining η for specific I from the $\pm 1/2 \leftrightarrow \pm 3/2$ transition features of Z-NQR, this graph has considerable significance. In contrast, the lineshape associated with $\pm 3/2 \leftrightarrow \pm 5/2$ transitions for $I=5/2$ exhibits little η-dependence.

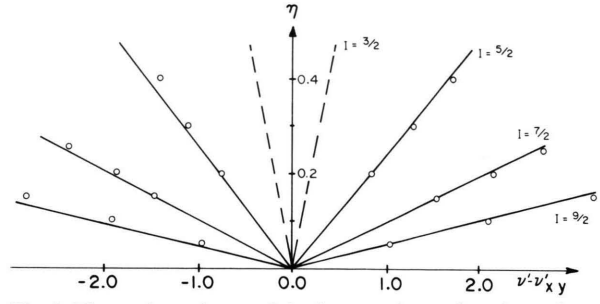

Fig. 9. The various slopes of the frequencies, as functions of η, $H \parallel \begin{pmatrix} x \\ y \end{pmatrix}$ orientations in the in four cases $I=3/2$, 5/2, 7/2 and 9/2. The frequency axis is in terms of ν' about a common origin at $\eta=0$; the actual origin for a specific I is given in Fig. 4 and in (12).

The Z-NQR Lineshape of $\pm 3/2 \leftrightarrow \pm 5/2$ Processes

As an example of an additional $\Delta m=1$ transition manifold involving higher pure-NQR states, we consider the $\pm 3/2 \leftrightarrow \pm 5/2$ Z-NQR transitions as a func-

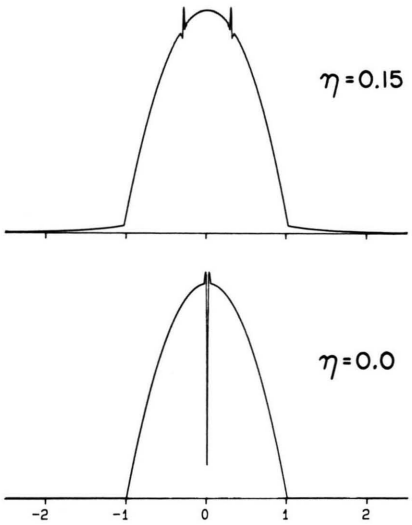

Fig. 10. The lineshapes for the $3/2 \leftrightarrow 5/2$ transitions of $I = 5/2$ at the two η values shown. These lineshapes are clearly of little value in estimating η in powder specimens.

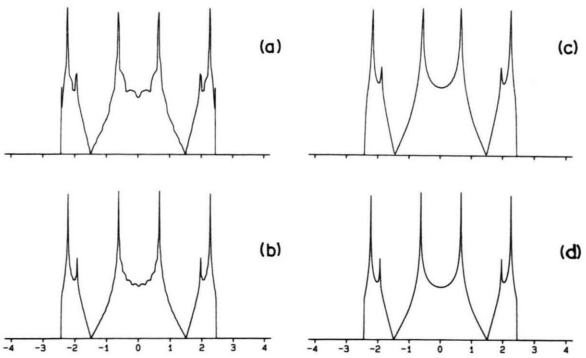

Fig. 11. Effect of varying the number of grid points N_G and the number of subdivisions of the frequency axis N_F, for $I = 5/2$, $\eta = 0.2$. Values of (N_F, N_G) are: (a) (1024, 8), (b) (1024, 16), (c) (256, 32), (d) (1024, 64). The spectrum (c) is almost identical to that calculated with the values (256, 64). The effect of increasing N_G is to remove the ripple apparent in (a) and (b). The effect of increasing N_F is to reduce the widths of the peaks and to increase the ratio of peak intensities to the intensities in the troughs; this can be seen by comparing (c) with (d).

tions of η. The corresponding lineshape, a broad intensity centred at $\nu' = 0$, is depicted in Figure 10. It is analogous to the central frequency region of the $I = 3/2$, $\pm 1/2 \leftrightarrow \pm 3/2$, $\eta = 0$ Z-NQR lineshape and lacks sufficient η-dependence to be useful in determining the asymmetry of the EFG tensor from experimental data.

Performance Characteristics of the Lineshape Algorithm

In addition to the optimization of the spherical averaging process previously discussed, it is useful to have some idea of the performance characteristics of the algorithm in respect to independent variation of the simulation parameters N_G and N_F, respectively the number of grid points and of frequency interval points. The actual quality, in respect of absence of 'ripple' or other artifacts, of the computed lineshape for specific $\{N_G, N_F\}$ choices is best seen by referring to Figs. 11 and 12, where an extended range of parameter sets have been utilized.

Estimates have been made of the functional dependence of the number of computational steps, n_c, involved in the simulation with N_G and N_F independantly varied, where the total computational time has been used to estimate n_c. It is found that

$$n_c \propto N_G^{3/2} N_F^{1/2} \tag{19}$$

and that reasonable quality lineshapes are obtainable in modest computational times for $N_F = 1024$, and $32 \leqq N_G \leqq 128$. The spectra in Figs. 7 and 8 with $N_G = 128$ each took approximately 12 minutes on an IBM P.C. with 8087 coprocessor.

Concluding Remarks

Comparison of the $1/2 \leftrightarrow 3/2$ processes with the analogous $3/2 \leftrightarrow 5/2$ transitions for $I = 5/2$ indicates that only the former are of direct utility in particular η determination. Further, the $\pm 1/2 \leftrightarrow \pm 3/2$ Z-NQR lineshapes exhibit distinct aspects which allow the $I = 3/2$ case, where $I = m'$ (see Fig. 1), to be contrasted with $I = 5/2$, or $I > 3/2$, cases. In particular, the central 'hump' maxima in the Z-NQR lineshape at $\nu = 0$ and low η values is a characteristic only of $m' = I$ systems. In contrast, in lineshapes associated with $I > m'$, the $\eta = 0$ spectra exhibit a pair of outer peaks originating from intensity contributions of the microcrystallite $H \parallel \bar{\theta}$ orientations where the special direction in the polar frame is governed solely by the magnitude of the quadrupolar spin, I. For $I = 3/2$ the $H \parallel \bar{\theta}$ conditions corresponds to the conventional NMR powder feature $H \parallel (z)$.

The focus of the graphical presentations has been concerned with investigations of the behaviour of the

$H \parallel \begin{pmatrix} x \\ y \end{pmatrix}$ features for specific spin I over a range of η values. Crossover of the $H \parallel \begin{pmatrix} x \\ y \end{pmatrix}$ features at the centre of the spectrum is found at $\eta = 1.00$, 0.335 and 0.185 for $I = 3/2$, $5/2$ and $7/2$, respectively. Whilst the enhanced sensitivity of these features to η variation for the $I \geqq 7/2$ is a striking phenomenon, it is wholly in accord with the early Bersohn-Toyama frequency expressions.

Criteria are established for choosing the two parameters associated with computational physics of powder lineshape calculations to give an optimal runtime. In addition, we note that in practical applications it is both convenient and feasible to calculate the individual 'inner' and 'outer' pair contributions to the $1/2 \leftrightarrow 3/2$ spectral manifold in separate lineshape simulations. Gaussian line-broadening of the lineshape can be readily incorporated by Fourier transform techniques.

In the context of the half-integer spin [5] and the single crystal Z-NQR frequency responses, we mention for completeness the existence of a time-domain formalism [17] which provides a theoretical description of quadrupolar spin-echo envelopes derived from Z-NQR pulse experiments.

Comparisons of measured Z-NQR spectra with calculations have been disappointing in the past. It is hoped to report on experimental work in subsequent publications.

Acknowledgements

This work was made possible by support from NSERC (Canada), which is gratefully acknowledged. The authors wish to express their appreciation of the continuing interest taken in this work by Dr. T. J. Bastow of C.I.R.S.O. Melbourne, Australia.

[1] M. Toyama, J. Phys. Soc. Japan, **14,** 1727 (1959).
[2] C. Dean, Phys. Rev. **96,** 1053 (1954).
[3] Y. Morino and M. Toyama, J. Chem. Phys. **35,** 1289 (1961).
[4] J. A. S. Smith and D. A. Tong, J. Chem. Soc. (A) 173 (1971).
[5] R. B. Creel and P. A. Drabold, J. Mol. Struct. **111,** 85 (1983).
[6] P. J. Bryant and S. Hacobian, Z. Naturforsch. **41 a,** 141 (1986).
[7] R. B. Creel, J. Magn. Reson. **52,** 515 (1983); et loc. cit.
[8] B. C. Sanctuary and S. M. Krishnan, Z. Naturforsch. **41 a,** 353 (1986); **42 a,** 907 (1987).
[9] G. M. Muha, J. Magn. Reson. **53,** 83 (1983).
[10] H. R. Brooker and R. B. Creel, J. Chem. Phys. **61,** 3658 (1974).
[11] S. Ramaprabbu and K. V. S. Rama Rao, Z. Naturforsch. **40 a,** 112 (1985).
[12] R. Ramachandran and E. Oldfield, J. Chem. Phys. **80,** 674 (1984).
[13] M. Goldman, Spin temperatures and NMR, Clarendon Press, Oxford 1970.
[14] M. A. Singh and R. L. Armstrong, J. Magn. Reson. **78,** 538 (1988).
[15] M. A. Singh and R. L. Armstrong, Phys. Rev. **B 38,** 50 (1988).
[16] D. W. Alderman, M. S. Solum, and D. M. Grant, J. Chem. Phys. **84,** 3717 (1986).
[17] N. E. Ainbinder and I. G. Shaposhnikov, in Adv. Nucl. Quadrupole Reson. **3,** 71 (1978).